



# Hollow WO<sub>3</sub>/SnO<sub>2</sub> Hetero-Nanofibers: Controlled Synthesis and High Efficiency of Acetone Vapor Detection

Hongyun Shao<sup>1,2</sup>, Minxuan Huang<sup>1,2</sup>, Hao Fu<sup>1,2</sup>, Shaopeng Wang<sup>1,2,3</sup>, Liwei Wang<sup>1,2,3\*</sup>, Jie Lu<sup>4\*</sup>, Yinghui Wang<sup>1,2</sup> and Kefu Yu<sup>1,2\*</sup>

<sup>1</sup> School of Marine Sciences, Guangxi University, Nanning, China, <sup>2</sup> Guangxi Laboratory on the Study of Coral Reefs in the South China Sea, Nanning, China, <sup>3</sup> Guangxi Key Laboratory of Processing for Nonferrous Metallic and Featured Materials, Nanning, China, <sup>4</sup> College of Life Science and Technology, Guangxi University, Nanning, China

## OPEN ACCESS

### Edited by:

Mingshui Yao,  
Kyoto University, Japan

### Reviewed by:

Xiaogan Li,  
Dalian University of Technology  
(DUT), China  
Fanli Meng,  
Northeastern University, China

### \*Correspondence:

Liwei Wang  
wangliwei0427@163.com  
Jie Lu  
jlu92@163.com  
Kefu Yu  
kefuyu@scsio.ac.cn

### Specialty section:

This article was submitted to  
Nanoscience,  
a section of the journal  
Frontiers in Chemistry

**Received:** 27 September 2019

**Accepted:** 31 October 2019

**Published:** 19 November 2019

### Citation:

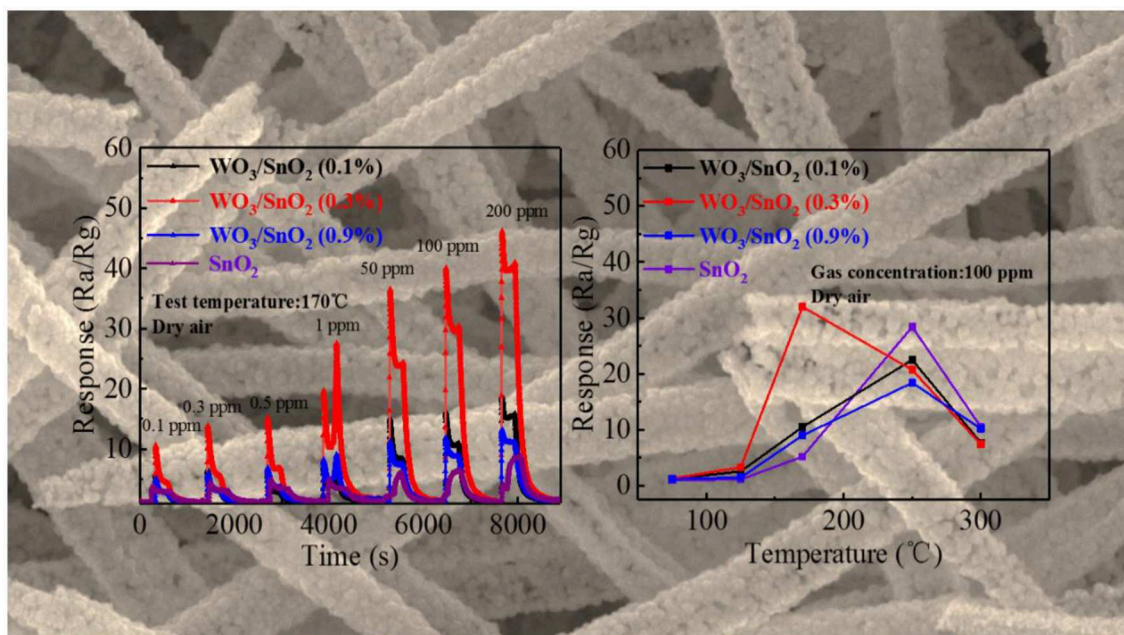
Shao H, Huang M, Fu H, Wang S, Wang L, Lu J, Wang Y and Yu K (2019) Hollow WO<sub>3</sub>/SnO<sub>2</sub> Hetero-Nanofibers: Controlled Synthesis and High Efficiency of Acetone Vapor Detection. *Front. Chem.* 7:785. doi: 10.3389/fchem.2019.00785

Metal oxide hetero-nanostructures have widely been used as the core part of chemical gas sensors. To improve the dispersion state of each constituent and the poor stability that exists in heterogeneous gas sensing materials, a uniaxial electro-spinning method combined with calcination was applied to synthesize pure SnO<sub>2</sub> and three groups of WO<sub>3</sub>/SnO<sub>2</sub> (WO<sub>3</sub> of 0.1, 0.3, 0.9 wt%) hetero-nanofibers (HNFs) in our work. A series of characterizations prove that the products present hollow and fibrous structures composed of even nanoparticles while WO<sub>3</sub> is uniformly distributed into the SnO<sub>2</sub> matrix. Gas sensing tests display that the WO<sub>3</sub>/SnO<sub>2</sub> (0.3 wt%) sensor not only exhibits the highest response (30.28) and excellent selectivity to acetone vapor at the lower detection temperature (170°C), 6 times higher than that of pure SnO<sub>2</sub> (5.2), but still achieves a considerable response (4.7) when the acetone concentration is down to 100 ppb with the corresponding response/recovery times of 50/200 s, respectively. Such structure obviously enhances the gas sensing performance toward acetone which guides the construction of a highly sensitive acetone sensor. Meanwhile, the enhancement mechanism of such a special sensor is also discussed in detail.

**Keywords:** electrostatic spinning, hollow nanofiber, WO<sub>3</sub>/SnO<sub>2</sub> heterojunction, acetone, gas sensor

## INTRODUCTION

The air quality in the workplace and living environment is closely related to people's health, it is therefore urgent to detect air pollution quickly and accurately. Acetone, a common organic volatile solvent, is widely used in laboratories and industries, posing a threat to the nose, eyes, and central nervous system of the human body when the concentration in the environment reaches 0.90 ppm (Hygienic Standard for Design of Industrial Enterprises) (Yang C. et al., 2019). Additionally, clinical data indicate that certain components of exhaust gases can be regarded as diagnostic markers of certain diseases, to that end acetone can be used as a marker of diabetes (Parthibavarman et al., 2018). Therefore, chemical gas sensors have emerged as many advantages such as portable, real-time and online detection are required (Meng et al., 2017; Yuan et al., 2019). Thus the development of acetone gas sensor can supply better service for safety control and human health (Meng et al., 2019).



**GRAPHICAL ABSTRACT** | Response curves of hollow WO<sub>3</sub>/SnO<sub>2</sub> hetero-nanofibers at different concentrations and temperatures.

To date, a great deal of research still focuses on fabricating high performance metal oxide semiconductor (MOS) gas sensing materials due to their many irreplaceable advantages such as their stability and their reliable sensing (Kucheyev et al., 2006; Das and Jayaraman, 2014; Yang and Guo, 2016; Teng et al., 2019), especially in improving the gas sensing properties of SnO<sub>2</sub>-based nanomaterials through the assembly into heterojunctions (Das and Jayaraman, 2014; Koohestani, 2019; Teng et al., 2019). It is known that pristine SnO<sub>2</sub>-based sensors often work at higher temperatures (>300°C) with poor selectivity, a lack of reproducibility, and an inadequate detection limit, thereby restricting their practical application (Wang et al., 2016; Wang L. et al., 2019). Hetero-junction constructing has become attractive since it produces intimate interface-contact directly between two different semiconductor materials, thus balancing the Fermi level, forming the thicker depletion layer on the interface, and finally increasing the sensor performances (Wang et al., 2016; Zhao et al., 2019).

Furthermore, SnO<sub>2</sub> composed of a hollow/porous nanostructure can help increase the surface area remarkably, and provide more channels to transfer electrons (Lu et al., 2011). 1D nanofibers (NFs) possess a high surface area-to-volume ratio, excellent stability, and can easily be modified which are favorable for enhancing response signals (Xia et al., 2010), while WO<sub>3</sub> has been widely studied in gas sensors with advantages of low temperature, high sensitivity, and low detection limit (Joshi et al., 2018; Li et al., 2018; Sukunta et al., 2018). By combining the advantages of 1D and hollow/porous structures, more attention is now being focused on the construction of the WO<sub>3</sub>/SnO<sub>2</sub> heterojunction. In comparison with other synthetic methods, like the hydrothermal or impregnation method, electro-spinning is the most effective method to uniformly control one-dimensional

hetero-nanofibers (HNFs) with a high yield and favorable stability (Ma et al., 2010; Wang et al., 2013).

Inspired by the newly reported 1D HNFs and with the intention of artificially tuning the gas-sensing performances, electro-spinning was used to construct hollow WO<sub>3</sub>/SnO<sub>2</sub> HNFs with different weight ratios of WO<sub>3</sub> (Patil et al., 2017; Wang K. et al., 2019). Herein, the synthesized sensor based on WO<sub>3</sub>/SnO<sub>2</sub> (0.3 wt%) could be a good candidate for acetone pollutant monitoring. Its gas sensing properties and working mechanism in particular will be evaluated and discussed systematically.

## EXPERIMENTAL SECTION

### Synthesis of Hollow WO<sub>3</sub>/SnO<sub>2</sub> HNFs

All the reagents used in the experiment, including Tin(II) chloride dehydrate (SnCl<sub>2</sub>·2H<sub>2</sub>O, AR, ≥98%), N,N-dimethylformamide (DMF, AR, 99.5%) and polyvinylpyrrolidone (PVP, K = 1300000, K88-96) were purchased from Aladdin Industrial Corporation (Shanghai, China). Sinopharm Chemical Reagent Co. Ltd. (Shanghai, China) provides ammonium tungstate hydrate ((NH<sub>4</sub>)<sub>10</sub>W<sub>12</sub>O<sub>41</sub>·xH<sub>2</sub>O, AR) and ethanol (CH<sub>3</sub>CH<sub>2</sub>OH, AR). Furthermore, distilled water was used in the synthesis procedures.

An electrostatic spinning method was applied for the preparation. Typically, 1 mmol of SnCl<sub>2</sub>·2H<sub>2</sub>O and a certain amount of (NH<sub>4</sub>)<sub>10</sub>W<sub>12</sub>O<sub>41</sub>·xH<sub>2</sub>O was dissolved in 2.32 ml of DMF and 2.79 ml of anhydrous ethanol under stirring. Then, 0.0003 mmol of PVP (K = 1300000) was added before the precursor solution was prepared. By controlling the amount of (NH<sub>4</sub>)<sub>10</sub>W<sub>12</sub>O<sub>41</sub>·xH<sub>2</sub>O, we designed different mass percentages of WO<sub>3</sub> as 0, 0.1, 0.3, 0.9 wt% respectively in the WO<sub>3</sub>/SnO<sub>2</sub> products, which were denoted as pure SnO<sub>2</sub>, WO<sub>3</sub>/SnO<sub>2</sub> (0.1%),

WO<sub>3</sub>/SnO<sub>2</sub> (0.3%), and WO<sub>3</sub>/SnO<sub>2</sub> (0.9%). Then the configured solution was transferred in the 5 ml syringe, then 20–22 kV of positive voltage was added to the needle and 3–4 kV of negative voltage to the receiver of the sample. The distance between the needles and the receiver was 15 cm, and the jet velocity of the fluid from the syringe was kept 2.32 mL of DMF and 2.79 mL as 0.2 mm/min under a high voltage electric field. In the whole electrostatic spinning process, the temperature was kept at 60°C and humidity of 10%. Afterwards, the white film was collected and calcined at 600°C, for 2 h in the air state, and finally different HNFs products were obtained.

## Characterization of Hollow WO<sub>3</sub>/SnO<sub>2</sub> HNFs

The samples were characterized by means of powder XRD analysis (Rigaku Ultima IV, Japan; Cu K $\alpha$  radiation,  $\lambda = 1.5418 \text{ \AA}$ ), Field-emission SEM (Hitachi SU5000, Japan), TEM and HRTEM with EDS (FEI Tecnai G2 f20 s-twin, 200 KV), XPS (Thermo SCIENTIFIC ESCALAB 250Xi, Al K $\alpha$  X-ray monochromator), BET (Autosorb-IQ, USA).

## Preparation of Gas Sensor and Sensing Test

The detailed manufacturing process of gas sensors can be found in our previous reports (Wang L. et al., 2019). Briefly, the sample was mixed with deionized water and ground until it became sticky and was then coated onto the surface of the ceramic tube, which was welded to the pedestal and inserted into the test channel. A gas-sensing test was carried out using the CGS-8 intelligent test system (Beijing Elite Tech Co. Ltd., China). The response value (*S*) of sensors based on n-type semiconductor is defined as  $S = R_a/R_g$ , where  $R_a$  and  $R_g$  represent the resistance value of the sensor in air and in target gas, respectively, while the p type is the opposite. Response time is defined as the time taken by the sensor to reach 90% of the final equilibrium value, or the recovery time for gas desorption. Most tests were carried out under dry air conditions, except the discussion of RHs effect on the response of different sensors (Xia et al., 2010; Wang et al., 2013; Wang L. et al., 2019).

## RESULTS AND DISCUSSION

### Characterization

X-ray diffraction was utilized to confirm the crystal structure of as-prepared samples. As shown in **Figure 1a**, the sharp diffraction peaks represent the pure tetragonal SnO<sub>2</sub> phase (JCPDS file No. 41-1445) with high crystallinity and large crystal size. Additionally, the main diffraction patterns in **Figures 1b–d** can also be indexed to tetragonal SnO<sub>2</sub>, but no obvious WO<sub>3</sub> peak presents due to its low content or highly dispersed amorphous state in the HNFs. Then the grain sizes of WO<sub>3</sub>/SnO<sub>2</sub> (0.1%, 0.3%, 0.9%) and pure SnO<sub>2</sub> samples were calculated by the Scherrer formula taken from  $2\theta = 26.6^\circ$  of the XRD data, which were 17.53, 15.71, 20.56, and 22.70 nm, respectively. It means that the grain size was smallest in the sample of WO<sub>3</sub>/SnO<sub>2</sub> (0.3%) HNFs. It is overwhelmingly known that when crystallite sizes approach Debye length ( $\lambda_D$ , usually several nm), the sensor

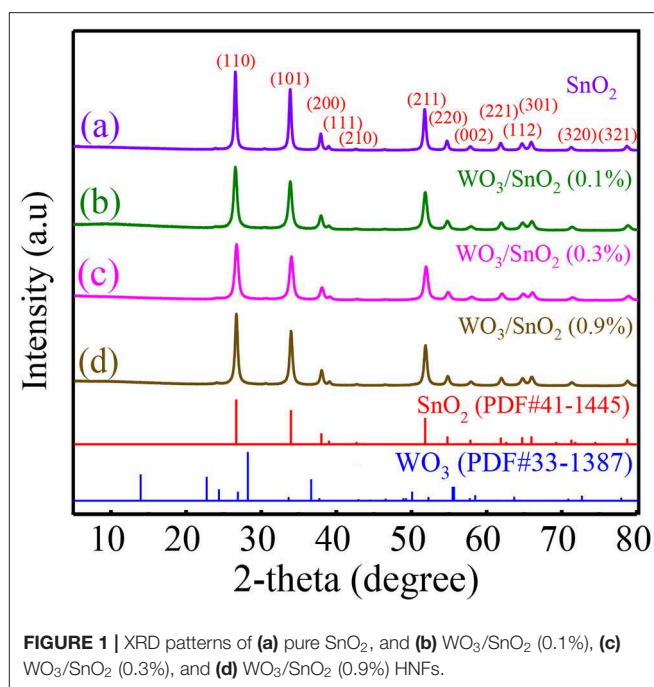
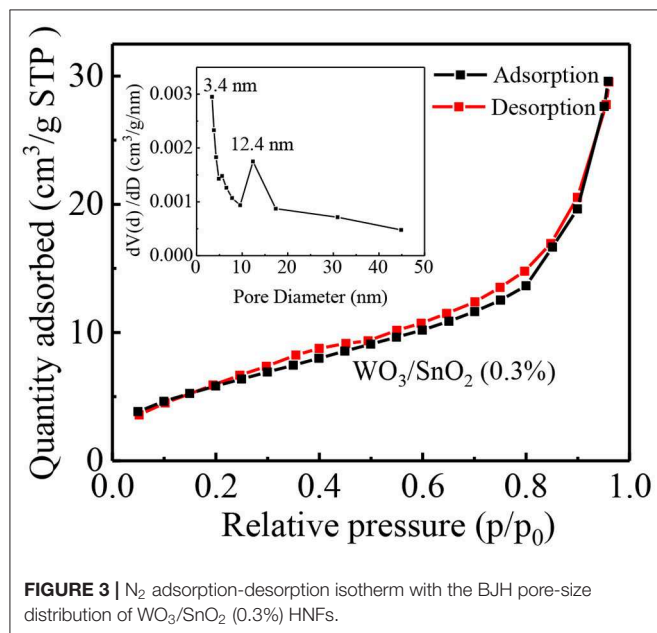
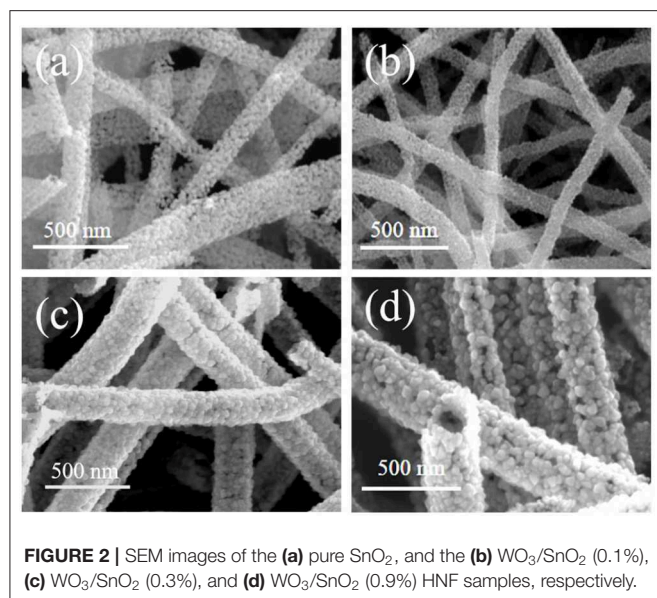


**FIGURE 1** | XRD patterns of (a) pure SnO<sub>2</sub>, and (b) WO<sub>3</sub>/SnO<sub>2</sub> (0.1%), (c) WO<sub>3</sub>/SnO<sub>2</sub> (0.3%), and (d) WO<sub>3</sub>/SnO<sub>2</sub> (0.9%) HNFs.

response will drastically increase, and the smaller the better (Miller et al., 2014; Nan et al., 2019). The conclusion can therefore be drawn from the XRD results that the WO<sub>3</sub>/SnO<sub>2</sub> (0.3%) sample with the smallest grain size, 15.71 nm, would exhibit excellent gas sensing performance in the following tests, and all the other characterizations were taken based on this example.

The morphology of each sample, namely the pure SnO<sub>2</sub>, and WO<sub>3</sub>/SnO<sub>2</sub> (0.1, 0.3, and 0.9%) HNF samples, respectively, were investigated by FESEM. As can be seen in **Figure 2a**, a uniform and hollow SnO<sub>2</sub> NF is composed of large numbers of nanoparticles with an average diameter of  $\sim 18$  nm, which is derived from the electro-spinning and heat treatment. Regarding the WO<sub>3</sub>/SnO<sub>2</sub> HNF samples in **Figures 2b–d**, they show similar morphologies to that of the pristine SnO<sub>2</sub> NF (**Figure 2a**), but as the amount of WO<sub>3</sub> increases, the average diameters of the particle-like construction units increase gradually to 22, 48, and 52 nm respectively. SEM results showed that the surface structure of SnO<sub>2</sub> NF had been changed by the doping of WO<sub>3</sub>, which may indirectly prove the existence of WO<sub>3</sub>. Such results are also proven through other investigations (HRTEM and XPS) in the following sections. Since the WO<sub>3</sub>/SnO<sub>2</sub> composite is comprised of aggregated nanoparticles with porous structures, the N<sub>2</sub> adsorption–desorption method (**Figure 3**) was applied on WO<sub>3</sub>/SnO<sub>2</sub> (0.3%) to confirm the speculation, as can be calculated from the data in **Figure 3** which shows that the specific surface area is 22.05 m<sup>2</sup>/g with a pore size diameter in the range of 3.4–45 nm averaged at 12.4 nm, proving its mesoporous structure for the composite. Therefore, the porosity of the sensing materials could improve its sensitivity due to the high surface area and rapid gas diffusion.

To more clearly provide insight into the microstructure, TEM & HRTEM were taken on the WO<sub>3</sub>/SnO<sub>2</sub> (0.3%) HNFs.



Corresponding to the SEM image in **Figure 4a**, the sample in the enlarged (**Figure 4b**) presents a hollow structure composed of various crossly-dispersed and stereoscopic nanofibers with width of  $\sim 200$  nm. In addition, it can be seen in **Figure 4c** that the interplanar spacings of the SnO<sub>2</sub> (110) and WO<sub>3</sub> (200) are 0.334 and 0.316 nm, respectively. The SAED pattern (**Figure 4d**) displays the polycrystal characteristic of the composite, while the elemental mapping shown in **Figures 4e–g** proves the existence of Sn, O and W elements in the final composite; in particular, W is uniformly distributed along the SnO<sub>2</sub> matrix. The corresponding EDS spectrum image and content of Sn, O and W elements were exhibited in **Figure S1**.

As is known, combining of the W element should bring interface change that then affects the chemical state of the SnO<sub>2</sub> substrate (Tang et al., 2014; Stojadinović et al., 2016). In order to obtain a clearer vision the elemental chemical status of pure SnO<sub>2</sub> and WO<sub>3</sub>/SnO<sub>2</sub> (0.9%) HNFs were confirmed by XPS in **Figure 5**. Besides the peaks of Sn, O and C, a tiny peak of W 4f can be seen in the XPS spectra of the WO<sub>3</sub>/SnO<sub>2</sub> (0.3%) composite (**Figures 5A,D**), consistent with the results shown in **Figure 4d**. The binding energy of Sn 3d<sub>3/2</sub> (494.98 eV) and Sn 3d<sub>5/2</sub> (486.58 eV) in particular, are displayed in the pure SnO<sub>2</sub>, but a minor negative shift of 0.18 eV can be noted for the Sn 3d<sub>3/2</sub> (494.8 eV) and Sn 3d<sub>5/2</sub> (486.4 eV) in the WO<sub>3</sub>/SnO<sub>2</sub> (0.3%) composite (**Figure 5B**) (Lavacchi et al., 2000; Liu et al., 2016). Furthermore, a minor negative shift of the binding energy is also observed for the element of O 1s (**Figure 5C**), i.e., the lattice oxygen [530.38 eV (O<sub>I</sub>)] and chemisorbed oxygen (531.24 eV (O<sub>II</sub>)) for pure SnO<sub>2</sub>, while 530.38 eV (O<sub>I</sub>) and 531.11 eV (O<sub>II</sub>) are the values for the WO<sub>3</sub>/SnO<sub>2</sub> (0.3%) composite, wherein the chemisorbed oxygen of O<sub>II</sub> shifts negatively for 0.13 eV (Yang and Guo, 2016; Yang C. et al., 2019). Note that the gas sensing property is quite relative to the content of chemisorbed oxygen which increases by 9% after W modification, so the sensing performance would be remarkably improved (Teng et al., 2019). Finally, in **Figure 5D**, W 4f in the WO<sub>3</sub>/SnO<sub>2</sub> (0.3%) composite gives a spin orbital dipole with two binding energies of 36.38 and 38.48 eV, respectively. The calculation results show that the spin orbit jet energy is 2.1 eV, which reaches a similar agreement with the theoretical calculation value (Nayak et al., 2015; Bai et al., 2016; Tofghi et al., 2019). According to the XPS results, interaction with the decoration of WO<sub>3</sub> is clearly witnessed, leading to the modification of the chemical state of the WO<sub>3</sub>/SnO<sub>2</sub> (0.3%) composite. In particular, the improved gas properties will be compared with pure SnO<sub>2</sub> and discussed in detail in the gas sensitivity test section.

## Gas Sensing Test

As mentioned, the WO<sub>3</sub>/SnO<sub>2</sub> (0.3%) HNF could be a good gas sensor candidate, since its hollow channel and porous structure may accelerate the gas diffusion and reaction on the active sites. Moreover, the interaction of W nanoparticles with the SnO<sub>2</sub> substrate can promote the O<sub>2</sub> chemisorption and generate a higher response when exposed to an acetone pollutant at low concentrations. Consequently, the optimal working temperature of the gas sensitive materials, based on various WO<sub>3</sub>/SnO<sub>2</sub> HNFs with acetone as the target gas was first determined with pure SnO<sub>2</sub> HNFs included for comparison. **Figure 6** shows that all the four response curves gradually increase when increasing the working temperature from 50°C, and decline at only 170°C for WO<sub>3</sub>/SnO<sub>2</sub> (0.3%), but 250°C for the other three samples. Additionally, the sensor that is based on WO<sub>3</sub>/SnO<sub>2</sub> (0.3%) provides the highest response (32) compared with other sensors. Just as expected, WO<sub>3</sub>/SnO<sub>2</sub> (0.3%) is a promising choice and all the following tests were carried out at the optimal operating temperature of 170°C.

Additionally, four dynamic response change curves of pure SnO<sub>2</sub> and WO<sub>3</sub>/SnO<sub>2</sub> sensor devices of different concentrations (0.1–200 ppm) of acetone at 170°C have been provided in

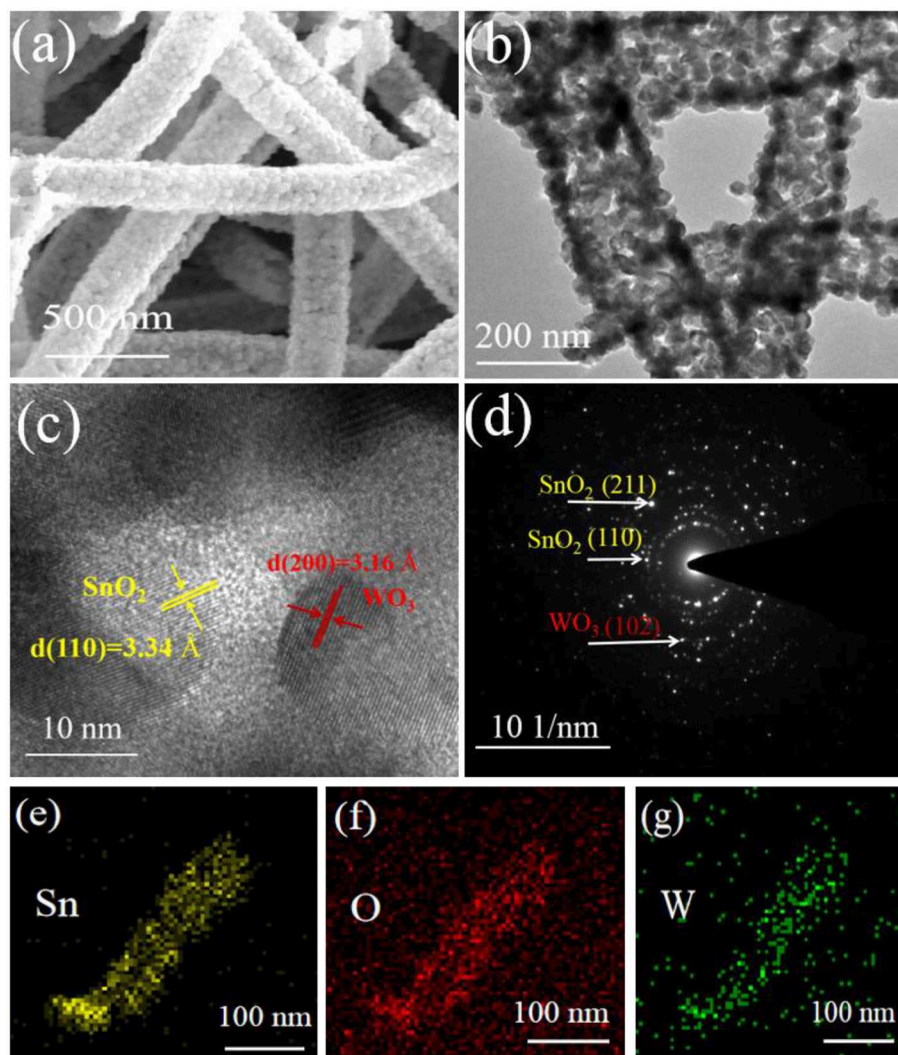


**FIGURE 4 |** (a) SEM image, (b) TEM image, (c) HRTEM image and (d) SAED of  $\text{WO}_3/\text{SnO}_2$  (0.3%) sample, with the (e–g) elemental mappings of Sn, O, and W elements.

**Figure 7.** As can be seen in **Figure 7A**,  $\text{WO}_3/\text{SnO}_2$  (0.3%) presents the highest response amplitude compared with the others, as well as the fastest instantaneous response speeds ( $\leq 6$  s), which proves its favorable response properties. (**Figure S3**) enlarged response–recovery curve for 100 ppb acetone gas was explored to determine the response/recovery time. At  $170^\circ\text{C}$ , for as-fabricated  $\text{WO}_3/\text{SnO}_2$  (0.3%) based sensor toward 100 ppb acetone gas, the response/recovery time was 50 and 200 s, respectively. Furthermore, the sensors display a better fold linear relationship between the response signal vs. acetone concentration (**Figure 7B**). Such a result clearly indicates that the gas sensitivity of  $\text{SnO}_2$  has been significantly improved through the synergistic effect of the hetero-junction formed by  $\text{WO}_3$  doping, which is also consistent with the results from **Figures 4, 5**. However, the doping amount of  $\text{WO}_3$  also displays an important role in the synergistic effect, thus affecting the surficial gas catalytic sensing properties.

In order to further confirm the selectivity of the  $\text{WO}_3/\text{SnO}_2$  (0.3%)-based sensor, 100 ppm of industrial gases such as methanol, formaldehyde, triethylamine, ethylenediamine and toluene were chosen to test at  $170^\circ\text{C}$ . **Figure 8A** shows that the  $\text{WO}_3/\text{SnO}_2$  (0.3%) sample not only exhibits excellent selectivity to acetone gas (32), three times more than other polluting gases, but also the highest response value compared to the other three sensors types. The sensor selectivity was influenced by many factors. On the one hand, the bond dissociation energy of  $\text{CH}_3\text{-COCH}_3$  (352 kJ/mol) is smaller than that of  $\text{C}_2\text{H}_5\text{O-H}$ ,  $\text{CH}_3\text{O-H}$  (462 kJ/mol),  $\text{H-COH}$  (368 kJ/mol),  $\text{H-CH}_2\text{C}_6\text{H}_5$  (371 kJ/mol), therefore, acetone is more likely to react with the adsorbed oxygen species than other gas molecules. On the other hand, the polar nature of the surface of the  $\text{WO}_3/\text{SnO}_2$  (0.3 wt%) would accelerate the adsorption of polar molecules. Acetone is much easier to be adsorbed on the surface of  $\text{WO}_3/\text{SnO}_2$  (0.3 wt%) than triethylamine. Consequently, more acetone molecules

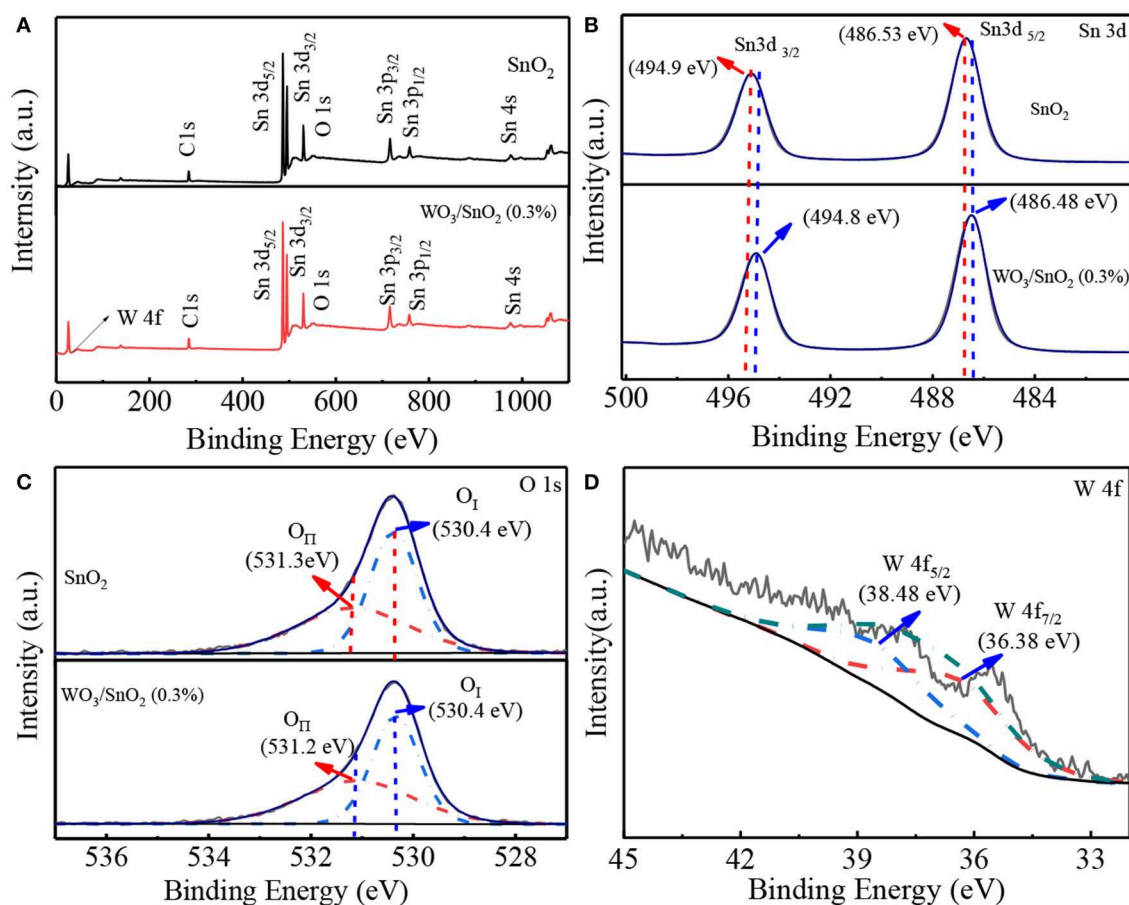


**FIGURE 5 |** (A) Survey spectra, and high magnification XPS spectra of (B) Sn 3d, (C) O 1s based on pure SnO<sub>2</sub> and WO<sub>3</sub>/SnO<sub>2</sub> (0.3%) HNF samples, as well as (D) W 4f in WO<sub>3</sub>/SnO<sub>2</sub> (0.3%) HNF, respectively.

can react with the adsorbed oxygen species which releases more electrons than any other gas molecule. As a result, the WO<sub>3</sub>/SnO<sub>2</sub> (0.3 wt%) hetero-nanofibers had a good sensing response and selectivity to acetone gas (Li et al., 2016; Zhang et al., 2017). The more detailed mechanism of adsorption and reaction using DFT calculation and *in situ* instruments, will be discussed in our future work. In **Figure 8B**, the corresponding desirable repeatability can also be witnessed for the four sensors to 100 ppm of acetone after five circles, especially the most attractive component of WO<sub>3</sub>/SnO<sub>2</sub> (0.3%). In general, the sensor based on WO<sub>3</sub>/SnO<sub>2</sub> (0.3%) HNF in this study is a promising candidate for trace indoor or industrial acetone gas sensing.

Last but not the least, to verify the stability of the prepared acetone sensor, the sensitivity of pure SnO<sub>2</sub> and three groups of WO<sub>3</sub>/SnO<sub>2</sub> (0.1, 0.3, 0.9 wt%) HNFs were detected every 6 days for 1 month. **Figure S2** shows that all the sensors nearly keep their response states, especially the sensor based on WO<sub>3</sub>/SnO<sub>2</sub> (0.3%) which exhibits quite high and stable response values. Such a result also indicates that the acetone gas sensor has good stability and prospective application.

To give a clear vision on the sensing properties of gas sensors to acetone, comparisons were made in **Table 1**. As can be seen, the gas sensor based on our WO<sub>3</sub>/SnO<sub>2</sub> (0.3%) HNF material displays the improved performance in a certain way, such as a lower working temperature of only 170°C. Generally, this work is valuable in enhancing the gas sensing properties by preparation of hollow hetero-structures.

### Gas Sensing Mechanism

The basic sensing principle for the n-type semiconductor metal oxides is based on the conductivity changes which are caused by surface gas adsorption and desorption (Wang Q. et al., 2019). In short, oxygen molecules in the air are adsorbed on the metal oxide surfaces. The different oxygen species including O<sup>-</sup>, O<sub>2</sub><sup>2-</sup>, and O<sub>2</sub><sup>-</sup> will form at different temperatures by capturing free electrons from the conduction bands of WO<sub>3</sub> and SnO<sub>2</sub>, e.g., the stable oxygen species on the surface of the sensing material is mainly O<sup>-</sup> below 300°C (Yamazoe et al., 2003; Rakshit et al., 2012). Thus, the electron concentration will be reduced to form an electron depletion layer, resulting in a higher resistance. When the sensor is exposed to the reduced gas like acetone, it can react with the adsorbed O<sup>-</sup> and release the captured electrons back,

thus decreasing the resistance (Das and Jayaraman, 2014; Yang and Guo, 2016).

On the basis of the above theory, the improved sensing performances for the sensor based on  $\text{WO}_3/\text{SnO}_2$  (0.3%) HNF can be attributed to three factors. First, as shown in **Figure 9**, the band gap and work function of  $\text{SnO}_2$  is 3.6 and 4.9 eV, while that for  $\text{WO}_3$  it is 2.6 and 4.8 eV, respectively. As the work functions of both are imbalanced, the electrons will transfer from the Fermi level of  $\text{WO}_3$  (higher Fermi level) to that of  $\text{SnO}_2$  (lower Fermi level) until they reach a balance, as displayed in **Figures 9A,B**. At the equilibrium point, the Schottky barrier with an additional depletion layer between  $\text{WO}_3$  and  $\text{SnO}_2$  are formed, controlling the electron transport efficiency of the

heterojunction (Rakshit et al., 2012; Koohestani, 2019). The  $\text{WO}_3/\text{SnO}_2$  hetero-structure provides more electrons to oxygen than pure  $\text{SnO}_2$ , then produces more  $\text{O}^-$  species on the materials surface. Therefore, the hetero-structure exhibits better sensing properties (Wal et al., 2009; Lingyue and Shantang, 2018; Yang et al., 2018).

Second, it's also the key factor that the synergetic effect between the interfaces can improve their sensing performances (Gu et al., 2011). It can be concluded from the TEM and XPS results in **Figures 4, 5** that,  $\text{WO}_3$  nanoparticles have been incorporated into the  $\text{SnO}_2$  HNFs successfully, thus both of them become highly accessible for the adsorption of oxygen species, add the thickness of the depletion layer at the interfaces and join in the reaction with acetone to a greater extent. This promotes the sensing response but helps reduce the working temperature of pure  $\text{SnO}_2$  (Parthibavarman et al., 2018; Wang L. et al., 2019). However, the heterojunctions with different contents of  $\text{WO}_3$  showed different gas sensing properties during the test, which also indicates that the optimal proportion of dopant is quite important in the construction of heterojunctions (Stojadinović et al., 2016).

The last factor has a lot to do with the morphology of the heterojunction. Many advantages exist in the HNFs produced by the electro-spinning method, since compared to the other three dimensions, the first characteristic of 1D nanostructure is its smaller dimension structure and high aspect ratio, which could efficiently transport electrical carriers along one controllable direction, making it highly suitable for moving charges in integrated nanoscale systems (Wal et al., 2009; Gu et al., 2011; Lu et al., 2011; Yuan et al., 2011; Wang et al., 2016). Additionally, the grain size also greatly affects the gas sensitivity. The region within a Debye length of the surface is known as the depletion region because it is depleted of its normal charge carriers. The Debye length may change to more or less when oxygen is adsorbed on the surface, which in turn causes a

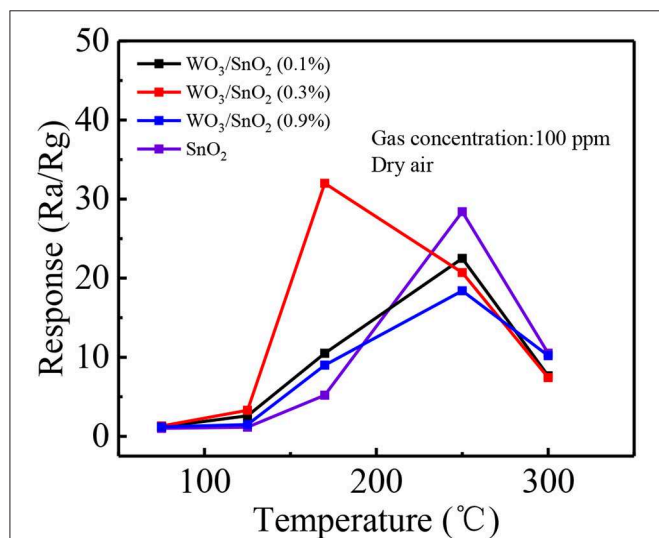


**FIGURE 6** | Response of the sensors based on above sensing materials to 100 ppm of acetone at operating temperatures from 50 to 300°C.

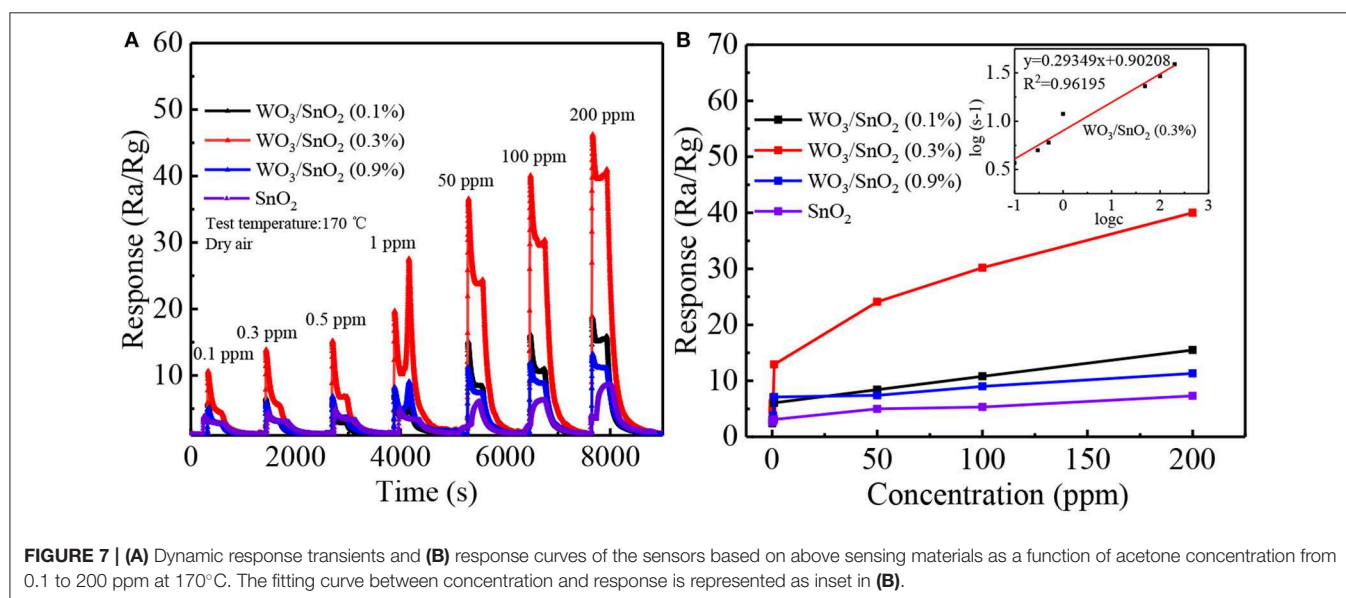


**FIGURE 7** | (A) Dynamic response transients and (B) response curves of the sensors based on above sensing materials as a function of acetone concentration from 0.1 to 200 ppm at 170°C. The fitting curve between concentration and response is represented as inset in (B).

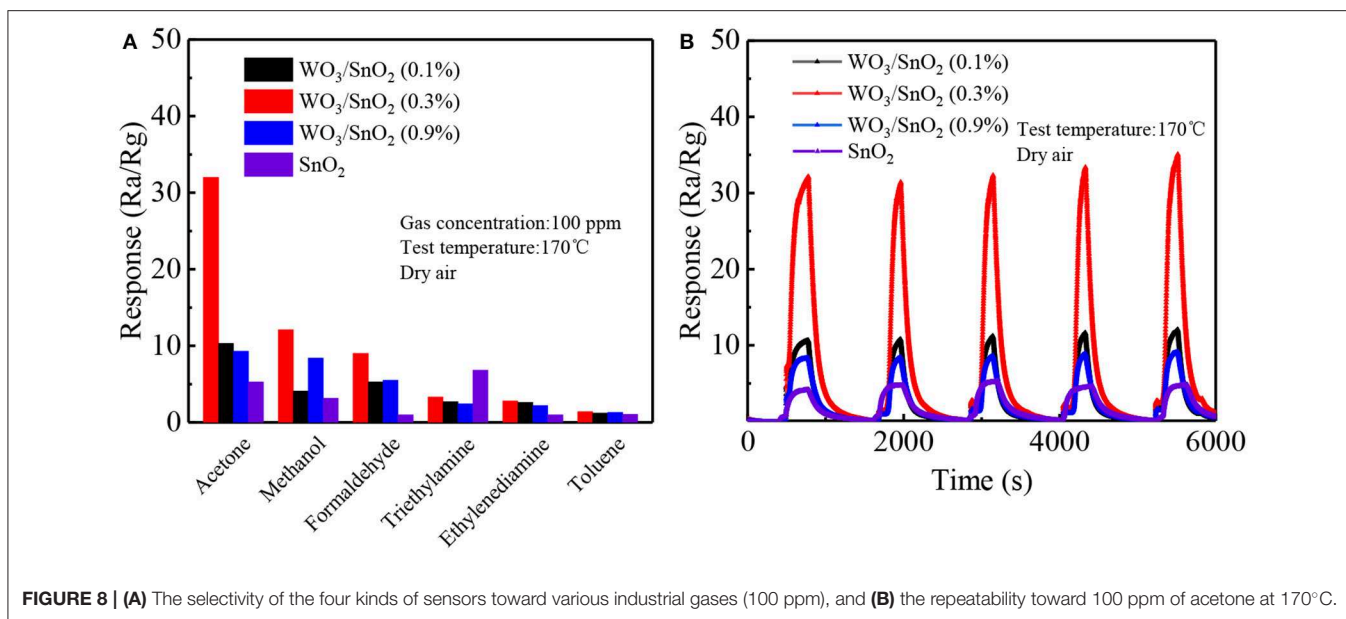
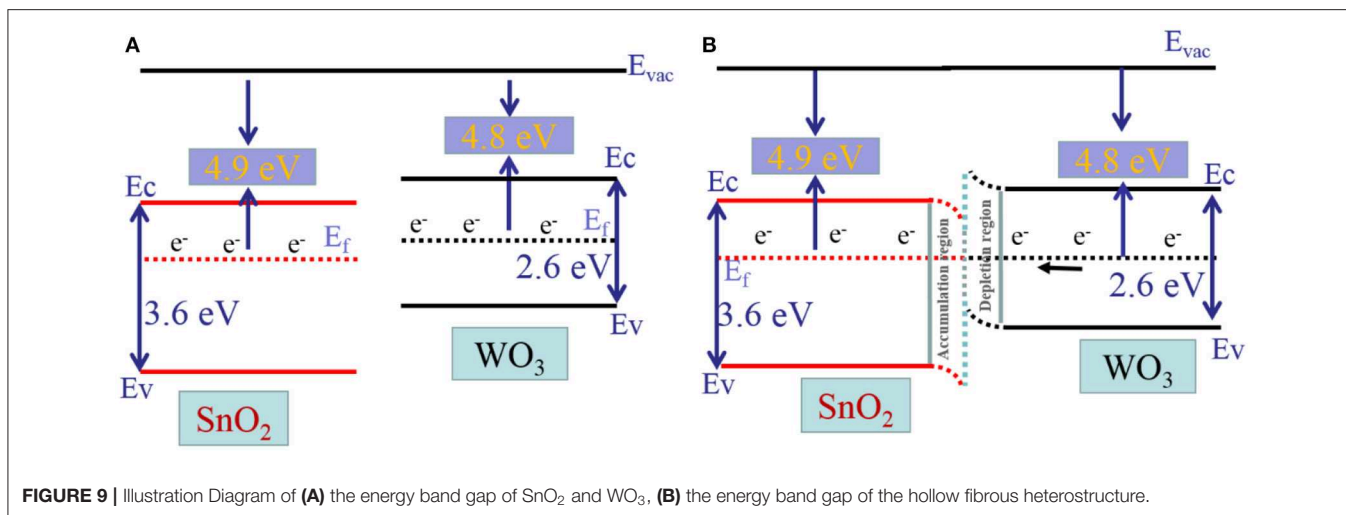


**TABLE 1 |** Sensing performance of various gas sensors toward acetone.

Materials	Method	W.T. (°C)	LOD (ppm)	Response	References
Ag@CuO-TiO <sub>2</sub>	Hydrothermal	200	1	11	Wang G. et al., 2019
Pt-decorated Fe <sub>2</sub> O <sub>3</sub> nanocubes	Hydrothermal	139	1	1.8	Zhang et al., 2019a
CoFe <sub>2</sub> O <sub>4</sub> nanoparticles (SM)	Solvothermal	220	50	16	Zhang H. et al., 2019
Porous NiFe <sub>2</sub> O <sub>4</sub> microspheres	Hydrothermal	250	0.2	1.2	Zhang et al., 2019b
0.5 wt% Au-ZnO	Sol-geltechnique	172	15	10	Yang M. et al., 2019
BiFeO <sub>3</sub> nanoparticles	Hydrothermal	350	1	1.8	Chakraborty and Pal, 2019
WO <sub>3</sub> /SnO <sub>2</sub> heterostructure	Electrospinning	170	0.1	4.7	This work



measurable change in the resistance. It has been overwhelmingly shown that when crystallite sizes are below about 20 nm, sensor response drastically increases (Miller et al., 2014), similar to the explanation presented in the XRD part, where the grain size calculations of various heterojunctions at 17.53, 15.71, and 20.56 nm in the  $\text{WO}_3/\text{SnO}_2$  (0.1%, 0.3%, 0.9%) composite, and the smallest grain size of 15.71 nm in the  $\text{WO}_3/\text{SnO}_2$  (0.3%), contributes to its best gas sensitivity among all the samples. The gas sensitivity was not controlled by the grain size of the main phase alone, but also the particle size, density, and distribution of the doped catalyst  $\text{WO}_3$ . As the doping amount of  $\text{WO}_3$  is 0.1 wt%, small  $\text{WO}_3$  nanoparticles are sparsely dispersed in  $\text{SnO}_2$  nanotubes with a lower density and less heterogeneous nodes. The increased charge carrier density would have little impact on depletion regions and the overall electrical conduction in the  $\text{WO}_3/\text{SnO}_2$  heterostructure. When the doping of  $\text{WO}_3$  is higher than 0.3 wt%, the crystallization of  $\text{WO}_3$  is accompanied by the growth of  $\text{SnO}_2$  crystallite size and the loss in specific surface area, leading to a less effective target gas diffusion, less reduction of depletion regions and deteriorated sensor response. Motivated by such facts, when the content of  $\text{WO}_3$  is above 0.3 wt% results in a weakened gas response.

## CONCLUSION

The heterogeneous structure and pure  $\text{SnO}_2$  of three components of  $\text{WO}_3/\text{SnO}_2$  hollow nanofibers (HNF) were prepared by electro spinning in this study. The grain size measured by TEM and calculated by scherer formula also proved that the group with the best gas sensitivity was  $\text{WO}_3/\text{SnO}_2$  (0.3%) HNF. Moreover, the large specific surface area characteristic of the hollow structure and the enhanced surface activity as the grain size decreases to the nanometer level providing a good way for the gas to enter the semiconductor material. The sample of the  $\text{WO}_3/\text{SnO}_2$  (0.3%) component has the best selectivity

## REFERENCES

- Bai, S., Guo, W., Sun, J., Li, J., Tian, Y., Chen, A., et al. (2016). Synthesis of  $\text{SnO}_2$ -CuO heterojunction using electrospinning and application in detecting of CO. *Sens. Actuators B*. 226, 96–103. doi: 10.1016/j.snb.2015.11.028
- Chakraborty, S., and Pal, M. (2019). Highly selective and stable acetone sensor based on chemically prepared bismuth ferrite nanoparticle. *J. Alloy. Compd.* 787, 1204–1211. doi: 10.1016/j.jallcom.2019.02.153
- Das, S., and Jayaraman, V. (2014).  $\text{SnO}_2$ : A comprehensive review on structures and gas sensors. *Prog. Mater. Sci.* 66, 112–255. doi: 10.1016/j.pmatsci.2014.06.003
- Gu, L., Zheng, K., Zhou, Y., Li, J., Mo, X., Patzke, G. R., et al. (2011). Humidity sensors based on ZnO/TiO<sub>2</sub> core/shell nanorod arrays with enhanced sensitivity. *Sens. Actuators B*. 159, 1–7. doi: 10.1016/j.snb.2010.12.024
- Joshi, N., Hayasaka, T., Liu, Y., Liu, H., Oliveira, O. N., and Lin, L. (2018). A review on chemiresistive room temperature gas sensors based on metal oxide nanostructures, graphene and 2D transition metal dichalcogenides. *Microchim. Acta* 185, 213–214. doi: 10.1007/s00604-018-2750-5
- Koohestani, H. (2019). Characterization of  $\text{TiO}_2/\text{WO}_3$  composite produced with recycled  $\text{WO}_3$  nanoparticles from W Ni Fe alloy. *Mater. Chem. Phys.* 229, 251–256. doi: 10.1016/j.matchemphys.2019.03.027
- Kucheyev, S. O., Baumann, T. F., Sterne, P. A., Wang, Y. M., Van Buuren, T., Hamza, A. V., et al. (2006). Surface electronic states in three-dimensional  $\text{SnO}_2$  nanostructures. *Phys. Rev. B*. 72, 1–5. doi: 10.1103/PhysRevB.72.035404
- for acetone in several representative industrial waste gases at the optimal operating temperature of 170°C. In particular, while the acetone concentration is as low as 100 ppb a good response was shown as well (4.7), and the response/recovery time was 50/200 s, respectively. This research can provide significant references for acetone gas sensors with low temperature and low detection limits.

## DATA AVAILABILITY STATEMENT

All datasets generated for this study are included in the article/**Supplementary Material**.

## AUTHOR CONTRIBUTIONS

HS initiated the experiments and draft. MH, HF, and SW helped prepare the samples. LW, JL, and KY contributed equally to this work, and they designed and completed the manuscript. YW offered useful comments on the technical methods.

## FUNDING

This work was funded by the National Natural Science Foundation of China (NO. 51762005, 91428203, and 61771267), Science and Technology Major Project of Guangxi (NO. AA17204074, AA17202020, AA17204100), and the Natural Science Foundation of Guangxi Province, China (2017GXNSFAA198254).

## SUPPLEMENTARY MATERIAL

The Supplementary Material for this article can be found online at: <https://www.frontiersin.org/articles/10.3389/fchem.2019.00785/full#supplementary-material>

- Lavacchi, C. B., Rovida, G., Bardi, U., Atrei, A., Angelucci, R., Dori, L., et al. (2000). Composition and structure of tin/vanadium oxide surfaces for chemical sensing applications. *Sens. Actuators B*. 71, 123–126. doi: 10.1016/S0925-4005(00)00596-7
- Li, F., Gao, X., Wang, R., and Zhang, T. (2018). Design of  $\text{WO}_3$ - $\text{SnO}_2$  core-shell nanofibers and their enhanced gas sensing performance based on different work function. *Appl. Surf. Sci.* 442, 30–37. doi: 10.1016/j.apsusc.2018.02.122
- Li, J., Tang, P., Zhang, J., Feng, Y., Luo, R., Chen, A., et al. (2016). Facile synthesis and acetone sensing performance of hierarchical  $\text{SnO}_2$  hollow microspheres with controllable size and shell thickness. *Ind. Eng. Chem. Res.* 55, 3588–3595. doi: 10.1021/acs.iecr.6b00060
- Lingyue, L., and Shantang, L. (2018). Oxygen vacancies as an efficient strategy for promotion of low concentration  $\text{SO}_2$  Gas Sensing: the case of Au modified  $\text{SnO}_2$ . *ACS Sustain. Chem. Eng.* 6, 13427–13434. doi: 10.1021/acssuschemeng.8b03205
- Liu, J., Xin, L., Xiang, C., Hao, N., Xiao, H., Zhang, T., et al. (2016). Synthesis of  $\text{SnO}_2/\text{In}_2\text{O}_3$  hetero-nanotubes by coaxial-electrospinning method for enhanced formaldehyde response. *New J. Chem.* 40, 1756–1764. doi: 10.1039/C5NJ02337H
- Lu, X., Zhang, W., Wang, C., Wen, T., and Wei, Y. (2011). One-dimensional conducting polymer nanocomposites: Synthesis, properties and applications. *Prog. Polym. Sci.* 36, 671–712. doi: 10.1016/j.progpolymsci.2010.07.010

- Ma, H., Yoon, K., Rong, L., Mao, Y., Mo, Z., Fang, D., et al. (2010). High-flux thin-film nanofibrous composite ultrafiltration membranes containing cellulose barrier layer. *J. Mater. Chem.* 20, 4692–4704. doi: 10.1039/b922536f
- Meng, F., Qin, W., Li, B., Zhang, H., Wang, S., Chang, Y., et al. (2019). Synthesis of Au nanoparticle-modified spindle shaped  $\alpha$ -Fe<sub>2</sub>O<sub>3</sub> nanorods and their gas sensing properties to N-butanol. *IEEE T Nanotechnol.* 18, 911–920. doi: 10.1109/TNANO.2019.2933569
- Meng, F., Zheng, H., Sun, Y., Li, M., and Liu, J. (2017). Trimethylamine sensors based on Au-modified hierarchical porous single-crystalline ZnO nanosheets. *Sensors* 17, 1–12. doi: 10.3390/s17071478
- Miller, D., R., and Akbar, S., A., Morris, P., A. (2014). Nanoscale metal oxide-based heterojunctions for gas sensing: a review. *Sens. Actuators B.* 204, 250–272. doi: 10.1016/j.snb.2014.07.074
- Nan, H., Guofeng, P., Jie, Z., and Ru, W. (2019). Co<sub>3</sub>O<sub>4</sub>-ZnO p-n Heterostructure low temperature acetone gas sensor. *Semicond. Technol.* 44, 379–385. doi: 10.13290/j.cnki.bdtjs.2019.05.010
- Nayak, A. K., Ghosh, R., Santra, S., Guha, P. K., and Pradhan, D. (2015). Hierarchical nanostructured WO<sub>3</sub>-SnO<sub>2</sub> for selective sensing of volatile organic compounds. *Nanoscale*. 7, 12460–12473. doi: 10.1039/C5NR02571K
- Parthibavarman, M., Karthik, M., and Prabhakaranc, S. (2018). Facile and one step synthesis of WO<sub>3</sub> nanorods and nanosheets as an efficient photocatalyst and humidity sensing material. *Vacuum* 155, 224–232. doi: 10.1016/j.vacuum.2018.06.021
- Patil, J. V., Mali, S. S., Kamble, A. S., Hong, C. K., Kim, J. H., and Patil, P. S. (2017). Electrospinning: a versatile technique for making of 1D growth of nanostructured nanofibers and its applications: an experimental approach. *Appl. Surf. Sci.* 423, 641–674. doi: 10.1016/j.apsusc.2017.06.116
- Rakshit, T., Mondal, S. P., Manna, I., and Ray, S. K. (2012). CdS-decorated ZnO nanorod heterostructures for improved hybrid photovoltaic devices. *ACS Appl. Mater. Inter.* 4, 6085–6095. doi: 10.1021/am301721h
- Stojadinović, S., Vasilčić, R., Radić, N., Tadić, N., Stefanov, P., and Grbić, B. (2016). The formation of tungsten doped Al<sub>2</sub>O<sub>3</sub>/ZnO coatings on aluminum by plasma electrolytic oxidation and their application in photocatalysis. *Appl. Surf. Sci.* 377, 37–43. doi: 10.1016/j.apsusc.2016.03.104
- Sukunta, J., Wisitorsaat, A., Tuantranont, A., Phanichphant, S., and Liewhiran, C. (2018). WO<sub>3</sub> nanotubes-SnO<sub>2</sub> nanoparticles heterointerfaces for ultrasensitive and selective NO<sub>2</sub> detections. *Appl. Surf. Sci.* 458, 319–332. doi: 10.1016/j.apsusc.2018.07.096
- Tang, W., Wang, J., Yao, P., and Li, X. (2014). Hollow hierarchical SnO<sub>2</sub>-ZnO composite nanofibers with heterostructure based on electrospinning method for detecting methanol. *Sens. Actuators B.* 192, 543–549. doi: 10.1016/j.snb.2013.11.003
- Teng, L., Liu, Y., Ikram, M., Liu, Z., Ullah, M., Ma, L., et al. (2019). One-step synthesis of palladium oxide-functionalized tin dioxide nanotubes: Characterization and high nitrogen dioxide gas sensing performance at room temperature. *J. Colloid. Interface Sci.* 537, 79–90. doi: 10.1016/j.jcis.2018.11.001
- Tofghi, G., Degler, D., Junker, B., Müller, S., Lichtenberg, H., Wang, W., et al. (2019). Microfluidically synthesized Au, Pd and AuPd nanoparticles supported on SnO<sub>2</sub> for gas sensing applications. *Sens. Actuators B.* 292, 48–56. doi: 10.1016/j.snb.2019.02.107
- Wal, R. L. V., Berger, G. M., Kulis, M. J., Hunter, G. W., Xu, J. C., and Laura, E. (2009). Synthesis methods, microscopy characterization and device integration of nanoscale metal oxide semiconductors for gas sensing. *Sensors-Basel*. 9, 7866–7902. doi: 10.3390/s91007866
- Wang, G., Fu, Z., Wang, T., Lei, W., Sun, P., Sui, Y., et al. (2019). A rational design of hollow nanocages Ag@CuO-TiO<sub>2</sub> for enhanced acetone sensing performance. *Sens. Actuators B.* 295, 70–78. doi: 10.1016/j.snb.2019.05.075
- Wang, K., Wei, W., Lou, Z., Zhang, H., and Wang, L. (2019). 1D/2D heterostructure nanofiber flexible sensing device with efficient gas detectivity. *Appl. Surf. Sci.* 479, 209–215. doi: 10.1016/j.apsusc.2019.02.094
- Wang, L., Fu, H., Jin, Q., Jin, H., Haick, H., Wang, S., et al. (2019). Directly transforming SnS<sub>2</sub> nanosheets to hierarchical SnO<sub>2</sub> nanotubes: towards sensitive and selective sensing of acetone at relatively low operating temperatures. *Sens. Actuators B.* 292, 148–155. doi: 10.1016/j.snb.2019.04.127
- Wang, Q., Bai, J., Huang, B., Hu, Q., Cheng, X., Li, J., et al. (2019). Design of NiCo<sub>2</sub>O<sub>4</sub>@SnO<sub>2</sub> heterostructure nanofiber and their low temperature ethanol sensing properties. *J. Alloy. Compd.* 791, 1025–1032. doi: 10.1016/j.jallcom.2019.03.364
- Wang, X., Ding, B., Sun, G., Wang, M., and Yu, J. (2013). Electro-spinning/netting: a strategy for the fabrication of three-dimensional polymer nano-fiber/nets. *Prog. Mater. Sci.* 58, 1173–1243. doi: 10.1016/j.pmatsci.2013.05.001
- Wang, Y., He, B., Wang, H., Xu, J., Ta, T., Li, W., et al. (2016). Transparent WO<sub>3</sub>/Ag/WO<sub>3</sub> electrode for flexible organic solar cells. *Mater. Lett.* 188, 107–110. doi: 10.1016/j.matlet.2016.11.054
- Xia, Y. N., Yang, P. D., Sun, Y. G., W. U. Y. Y., Mayers, B., Gates, B., et al. (2010). One-dimensional nanostructures: synthesis, characterization, and applications. *Adv. Mater.* 15, 353–389. doi: 10.1002/adma.200390087
- Yamazoe, N., Sakai, G., and Shimanoe, K. (2003). Oxide semiconductor gas sensors. *Catal. Surv. Asia*. 7, 63–75. doi: 10.1023/A:1023436725457
- Yang, C., Miao, G., Pi, Y., Xia, Q., Wu, J., Li, Z., et al. (2019). Abatement of various types of VOCs by adsorption/catalytic oxidation: a review. *Chem. Eng. J.* 370, 1128–1153. doi: 10.1016/j.cej.2019.03.232
- Yang, F., and Guo, Z. (2016). Tuning SnO<sub>2</sub> architectures with unitary or composite microstructure for the application of gas sensor. *J. Colloid Interface Sci.* 462:140–147. doi: 10.1016/j.jcis.2015.09.074
- Yang, M., Zhang, S., Qu, F., Gong, S., Wang, C., Qiu, L., et al. (2019). High performance acetone sensor based on ZnO nanorods modified by Au nanoparticles. *J. Alloy. Compd.* 797, 246–252. doi: 10.1016/j.jallcom.2019.05.101
- Yang, W., Feng, L., He, S., Liu, L., and Liu, S. (2018). Density gradient strategy for preparation of broken In<sub>2</sub>O<sub>3</sub> microtubes with remarkably selective detection of triethylamine vapor. *ACS Appl. Mater. Interfaces* 10, 27131–27140. doi: 10.1021/acsami.8b09375
- Yuan, J., Xu, Y., and A., Müller, H. E. (2011). One-dimensional magnetic inorganic-organic hybrid nanomaterials. *Chem. Soc. Rev.* 40, 640–655. doi: 10.1039/c0cs00087f
- Yuan, Z., Zhao, J., Meng, F., Qin, W., Chen, Y., Yang, M., et al. (2019). Sandwich-like composites of double-layer Co<sub>3</sub>O<sub>4</sub> and reduced graphene oxide and their sensing properties to volatile organic compounds. *J. Alloy. Compd.* 793, 24–30. doi: 10.1016/j.jallcom.2019.03.386
- Zhang, H., Liu, L., Zhang, X., Zhang, S., and Meng, F. (2019). Microwave-assisted solvothermal synthesis of shape-controlled CoFe<sub>2</sub>O<sub>4</sub> nanoparticles for acetone sensor. *J. Alloy. Compd.* 788, 1103–1112. doi: 10.1016/j.jallcom.2019.03.009
- Zhang, S., Jiang, W., Li, Y., Yang, X., Sun, P., Liu, F., et al. (2019b). Highly-sensitivity acetone sensors based on spinel-type oxide (NiFe<sub>2</sub>O<sub>4</sub>) through optimization of porous structure. *Sens. Actuators B.* 291, 266–274. doi: 10.1016/j.snb.2019.04.090
- Zhang, S., Song, P., Zhang, J., Yan, H., Li, J., Yang, Z., et al. (2017). Highly sensitive detection of acetone using mesoporous In<sub>2</sub>O<sub>3</sub> nanospheres decorated with Au nanoparticles. *Sens. Actuators B.* 242, 983–993. doi: 10.1016/j.snb.2016.09.155
- Zhang, S., Yang, M., Liang, K., Turak, A., Zhang, B., Meng, D., et al. (2019a). An acetone gas sensor based on nanosized Pt-loaded Fe<sub>2</sub>O<sub>3</sub> nanocube. *Sens. Actuators B.* 290, 59–67. doi: 10.1016/j.snb.2019.03.082
- Zhao, S., Shen, Y., Zhou, P., Zhong, X., Han, C., Zhao, Q., et al. (2019). Design of Au@WO<sub>3</sub> core-shell structured nanospheres for ppb-level NO<sub>2</sub> sensing. *Sens. Actuators B.* 282, 917–926. doi: 10.1016/j.snb.2018.11.142

**Conflict of Interest:** The authors declare that the research was conducted in the absence of any commercial or financial relationships that could be construed as a potential conflict of interest.

Copyright © 2019 Shao, Huang, Fu, Wang, Wang, Lu, Wang and Yu. This is an open-access article distributed under the terms of the Creative Commons Attribution License (CC BY). The use, distribution or reproduction in other forums is permitted, provided the original author(s) and the copyright owner(s) are credited and that the original publication in this journal is cited, in accordance with accepted academic practice. No use, distribution or reproduction is permitted which does not comply with these terms.